Analysis, Design and Implementation of a Quasi-Proportional-Resonant Controller for Multi-functional Capacitive-Coupling Grid-Connected Inverter

Tao Ye[1], NingYi Dai[1], Chi-Seng Lam[1,2], Man-Chung Wong[1], Josep M. Guerrero[3]

1. Electrical and Computer Engineering Department, University of Macau, Macao, P.R. China
2. State Key Laboratory of Analog and Mixed-Signal VLSI, University of Macau, Macao, China
3. Department of Energy Technology, Aalborg University, Denmark

***Abstract*—The capacitive-coupling grid-connected inverter (CGCI) is able to achieve reactive power compensation and active power transfer simultaneously with a low operational voltage. The CGCI is coupled to the point of common coupling (PCC) via a second-order LC circuit, which makes its modeling and current control characteristics differs from the conventional inductive-coupling grid-connected inverter. The direct current tracking with hysteresis pulse width modulation (PWM) was used in previous studies. However, this method suffers from widely varying switching frequency and large current ripples. A Quasi-proportional-resonant (Quasi-PR) current controller is designed for the CGCI in this paper. Its modeling and parameter selection are studied in detail. In contrast with proportional-integration (PI) current controller, the Quasi-PR controller reduces steady-state error. It also generates a voltage reference for applying the carrier-based PWM to improve output waveform quality. Simulation results are provided to verify the Quasi-PR controller and comparison with the PI controller is also done. A lab-scale prototype is built. Experimental results are given to show the validity of the proposed control method and its design.**

***Keywords*—Capacitive-coupling grid connected inverter; Quasi-PR controller; Proportional-integration controller; parameters design**

I. INTRODUCTION

The increasing need for more effective and environmental friendly power electrical system plays an active role in the development of smart grid [1-4]. Grid-connected inverter is the key for efficient use of distributed energy resources. Recently, more and more attention has been paid to multifunctional grid-connected inverters, which provide auxiliary services on power quality enhancement [5-6]. Most of the inverter is coupled to the grid via L type, LC type or LCL type filter. They are named as inductive-coupling grid-connected inverters (IGCI) in this paper [7-9].

The capacitive-coupling grid-connected inverter (CGCI) was proposed and used to achieve the same function [10-11].The configuration of a single-phase CGCI is shown in Fig. 1. The CGCI is integrated to the grid via an inductor in series with a capacitor. This topology is first proposed with the name of hybrid filter [12-13]. It is named capacitive since the fundamental frequency impedance of its coupling branch is capacitive [14]. The capacitive coupling branch reduces the operational voltage of the CGCI when leading reactive power is injected to the grid [15]. By adding active power transfer capability to the CGCI, the previous research work shows that it is a promising low-cost alternative to existing IGCI.

The direct current tracking with hysteresis PWM was used to control CGCI in previous work since it is simple and easy to implement [10,11]. The hysteresis PWM method has the drawbacks of widely varying switching frequency and large current ripples. The carrier-based PWM is able to fix switching frequency and reduce output current distortion. A current controller is used to generate voltage reference for applying carrier-based PWM in conventional IGCI. Proportional-integrator (PI) and proportional-resonant (PR) are the two most widely used current controller [16-18]. However, conventional PI controller is not able to eliminate steady-state errors in current tracking [19]. Synchronous PI controller was proposed for three-phase IGCI, in which stationary-frame ac quantities are transformed to dc quantities [20]. In this way, to achieve theoretical zero steady-state errors is then possible. However, additional computations are required for coordinate transformation when this method is applied to single-phase IGCI.

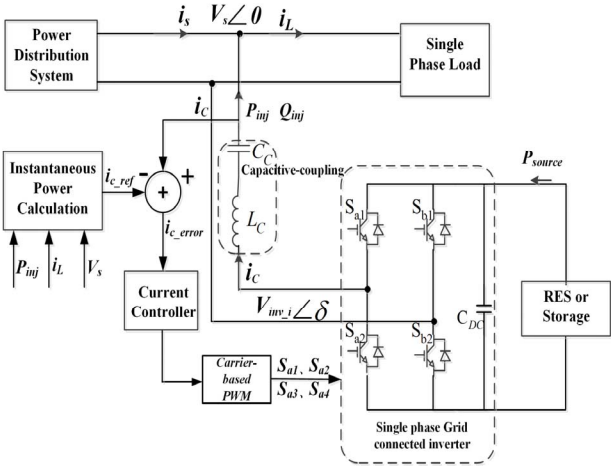

Fig. 1 System configuration of a single-phase CGCI

A stationary-frame PR controller has the same operational principal as a synchronous-frame PI controller when it is applied to a single-phase IGCI [21,22]. Compared to a stationary-frame PR controller, Quasi-PR controller avoids the stability problems associated with an infinite gain and can reduce sensitivity towards slight frequency variation in a typical utility grid [23,24]. Through comparing pros and cons of different current controllers for IGCI, a Quasi-PR current controller is selected and will be applied to control CGCI in this paper. The frequency response of the grid-connected inverter is studied and parameters design of the Quasi-PR current controller for the CGCI will be proposed in this paper. In Section II, the operational principal of the CGCI is introduced and its mathematical model is built and analyzed. The parameter design of the Quasi-PR controller is presented in Section III. Comparison with the PI current controller is also given in this Section. Simulation results are given in Section IV. Experimental results are provided in Section V.

II. MODELING OF THE CGCI

A. Operational principal of the CGCI

The system configuration of CGCI is shown in Fig. 1. It is integrated to the grid via an inductor in series with a capacitor. The power flow between the inverter and the grid can be calculated as shown below, following [25].

$$P_{inj} = \left(\frac{V_s V_{inv}}{Z} \cos\delta - \frac{V_s^2}{Z} \right) \cos\theta + \frac{V_s V_{inv}}{Z} \sin\delta \cdot \sin\theta \quad (1)$$

$$Q_{inj} = \left(\frac{V_s V_{inv}}{Z} \cos\delta - \frac{V_s^2}{Z} \right) \sin\theta - \frac{V_s V_{inv}}{Z} \sin\delta \cdot \cos\theta \quad (2)$$

In (1) and (2), V_{inv} is the output voltage of the inverter; and δ represents the phase angle between V_s and V_{inv}. The value of $Z\angle\theta$ and θ is determined by the coupling impedance of the grid-connected inverter. The impedance of the coupling branch in CGCI is expressed as follows.

$$X_c = Z\angle\theta = -j\frac{1}{\omega C_c} + j\omega L_c = -j\frac{1}{\omega C} = \frac{1}{\omega C}\angle -90^\circ \quad (3)$$

The power base is introduced as follows.

$$S_{base} = V_s^2 \cdot \omega C \quad (4)$$

By combining (1) to (4), the normalized output voltage of the CGCI is calculated as shown in (5), and its variation in power flow is depicted in three dimensions (3D) in Fig. 2.

$$\frac{V_{inv}}{V_s} = \sqrt{\left(\frac{P_{inj}}{S_{base}}\right)^2 + \left(\frac{Q_{inj}}{S_{base}} - 1\right)^2} \quad (5)$$

It can be concluded from Fig. 2 that the operational voltage of the inverter is lower than the grid voltage when the reactive power is in the vicinity of S_{base}. The CGCI is better to be connected to a PCC, where continuous reactive power compensation is required for inductive loadings, for example, pumps or air-conditioners installed on the roof top.

As a multifunctional grid-connected inverter, the CGCI is able to transfer active power from the renewable energy sources to the grid and compensate reactive power and harmonics at the PCC simultaneously. The simplified block diagram of the control system for the CGCI is given in Fig.3, in which a current controller is used to provide reference for the carrier-based PWM unit. The carrier-based PWM method is selected due to its fixed switching frequency, low current ripples, and well defined harmonic spectrum characteristics.

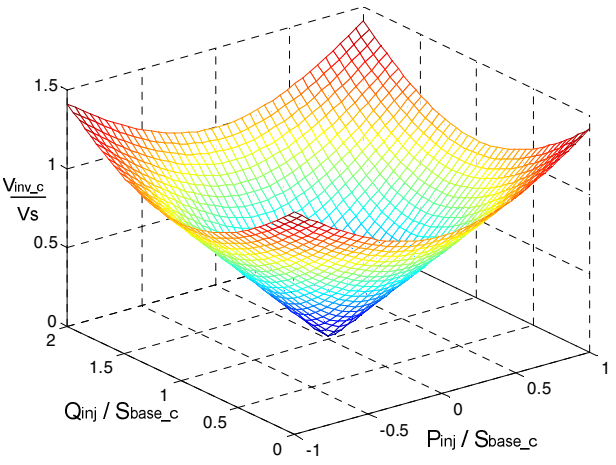

Fig. 2 Variation in inverter voltage with power

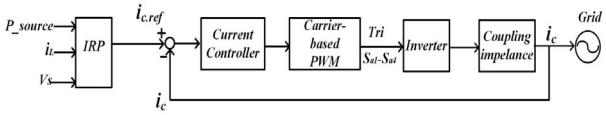

Fig. 3 Control block diagram of Grid-Connected inverter

The output current reference can be calculated by:

$$i_{c\_ref} = \frac{1}{v_m^2}\begin{bmatrix}\sin\theta & \cos\theta\end{bmatrix}\begin{bmatrix}p_{source} + \tilde{p}_L \\ q_L\end{bmatrix} \quad (6)$$

Where P_{source} represents the active power from distributed generators. The load power is extracted by using instantaneous reactive power theory, as discussed in previous work [10,11].

B. Modeling of CGCI with a current controller

To analysis and design the control system in Fig. 3, a model is deduced, as given in *Fig. 4*. There are mainly three blocks in *Fig. 4*: current controller, PWM-controlled inverter and coupling branch. The detailed mathematical model of each block is discussed hereinafter.

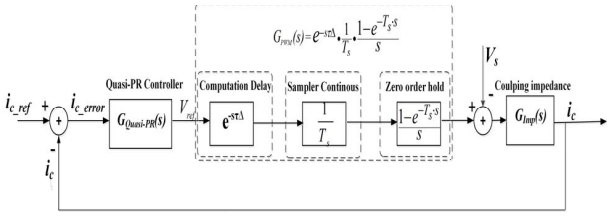

Fig. 4 S-domain control model

- Current Controller

As mentioned in Section I, Quasi-PR controller is selected in this paper. Its transfer function, $G_{Quasi\text{-}PR}(s)$ is as follows.

$$G_{Quasi-PR}(s)=K_p+\frac{2K_r\omega_c s}{s^2+2\omega_c s+\omega_0^2} \quad (7)$$

- PWM Unit

In an average s-domain model, the PWM converter may be simplified to a unity gain. However, the computation time of the digital controller is not negligible [26-29]. In order to accurately describe the real effects of time delay, the sampler and the zero-order hold, a s-domain PWM unit model is used as given in *Fig. 4*. The s-domain transfer function of the PWM converter is expressed as

$$G_{PWM}(s)=D(s)=\frac{e^{-T_s\cdot s}(1-e^{-T_s\cdot s})}{T_s\cdot s} \quad (8)$$

Where T_s is the sampling period.

In order to obtain rational transfer functions, delays are usually approximated by poles and zeros. A proper way is to use the *Pade′* approximation, and the first order *Pade′* approximation shown in (9) maintains the S-domain analysis with a fair agreement between simplicity and accuracy.

$$e^{-T_s\cdot s}\approx\frac{1-0.5\cdot T_s\cdot s}{1+0.5\cdot T_s\cdot s}=Pade' \quad (9)$$

Substitute (9) into formula (8) and it can get:

$$G_{PWM}(s)=\frac{e^{-T_s\cdot s}(1-e^{-T_s\cdot s})}{T_s\cdot s}\approx\frac{1-0.5\cdot T_s\cdot s}{(1+0.5\cdot T_s\cdot s)^2} \quad (10)$$

- Coupling impedance

The LC coupling branch of the CGCI is expressed as following.

$$G_{Imp}(s)=\frac{C_c s}{L_c C_c S^2+1} \quad (11)$$

According to *Fig. 4*, the overall transfer function is obtained as following:

$$\begin{aligned} I_c(s) &= G_{cref\_c}I_{c\_ref}(s)-G_{vs\_c}V_s(s) \\ &= \frac{G_{Quasi-PR}(s)G_{PWM}(s)G_{Imp}(s)}{1+G_{Quasi-PR}G_{PWM}(s)G_{Imp}(s)}I_{c\_ref}(s) \\ &\quad -\frac{G_{Imp}(s)}{1+G_{Quasi-PR}G_{PWM}(s)G_{Imp}(s)}V_s(s) \end{aligned} \quad (12)$$

$G_{cref\_c}(s)$ is the system closed-loop transfer function between i_c and i_{c_ref}, and $G_{vs\_ic}(s)$ is the closed-loop system transfer function between i_c and V_s. Besides, $G_{Quasi-PR}(s)G_{PWM}(s)G_{Imp}(s)$ is the open-loop transfer function

III. Parameter Design of the Quasi-PR Controller

A. Parameters design of Quasi-PR Controller in CGCI

The performance of the CGCI is greatly affected by the current controller. There are mainly three parameters need to be selected in order to implement a quasi-PR current controller [30,31]. Design scenario can be summarized to this:

- An appropriate ω_c should be chosen to give a satisfactory bandwidth around the resonant frequency.
- K_p should be chosen such that good transient response and stability are guaranteed.
- K_r is chosen so that phase and magnitude steady state errors are eliminated.

On the basis of the power quality standard of Macau and Hong Kong (HKE and CLP supply rules of Hong Kong, CEM supply rules), the standard limit of frequency variation is ±2%. Assuming that the frequency variation margin is ±2%, then ω_c=2*π*50*2%=6.28.

K_p should be large enough to obtain high gain at the fundamental frequency and low-order harmonic frequency. However, larger K_p makes the system less stable. Using Quasi-PR controller can overcome this problem. It provides high value gain at the fundamental frequency and low-order harmonic frequency with relatively small K_p value.

The boundary of the K_p value is determined by using Routh's stability criterion. The open loop transfer function of related closed-loop transfer function $G_{cref\_c}(s)$ is $G_{Quasi-PR}(s)G_{PWM}(s)G_{Imp}(s)=N(s)/D(s)$. Then the characteristic equation can be obtained from:

$$D(s)+KN(s)=0 \quad (13)$$

It is assumed the delay time of the PWM unit is half a sampling period ($0.5T_s$), the corresponding boundary of K_p are deduced as follows:

$$K_p\le(8\cdot L_c)/(3\cdot T_s) \quad (14)$$

It can be concluded from (12) that the magnitude gain of $G_{Quasi-PR}(s)G_{PWM}(s)G_{Imp}(s)$ needs to be higher than 100 in order to decrease the current tracking error to below 1%. The value of K_r and K_p are selected to satisfy this requirement and to guarantee stable operation and acceptable transient response at the same time.

The design procedure of the Quasi-PR controller for a CGCI is as following:

1) According to the power quality standard to select the value of ωc.

$$\omega_c=2\cdot\pi\cdot f_0\cdot\Delta f \quad (15)$$

Where f_0 is the fundamental frequency and Δf is the standard limit of the frequency variation.

2) Calculate the upper boundary (106.7) of the controller's proportional gain K_p according to (14). Select a value of K_p within this boundary.

3) Set a small value for K_r, which can guarantee the magnitude response of the open-loop transfer function at the designed resonant frequency (50Hz) is above 40 dB.

4) Adjust K_p value within its boundary so that The magnitude response of closed-loop transfer function $G_{cref\_c}(s)$ approaches to 0 dB and its phase response curve approaches to 0 degree at fundamental frequency.

5) The value of K_r and ω_c may need minor adjustments to fulfill the following requirements:

- The magnitude response of the closed-loop transfer function $G_{cref\_c}(s)$ should be close to the 0 dB for low-order harmonic frequencies.
- K_r is adjusted to make sure that the magnitude response at high frequency especially around 10 KHz are well suppressed.

B. Parameters design Verifications

Current controller model is analyzed by using Matlab. The system settings are given in Table. I. The bode diagram of open-loop current controller and closed-loop current control system is shown in Figs. 5 and 6, respectively. Results indicate that $G_{cref\_c}(s)$ has a unity gain with zero phase shifting at fundamental frequency with the selected parameters.

C. Comparison of PI controller controlled CGCI and Quasi-PR controller controlled CGCI system

Comparison with PI controller is done in this section. PI controller is one of the most widely use current tracking controller for grid-connected inverter. The PI controller is expressed as follows:

$$G_{PI}(s) = K_p + \frac{K_i}{s} \tag{16}$$

By using (16) to replace $G_{quasi\text{-}PR}(s)$ in (12), the S-domain transfer function with PI controller is obtained.

With the parameters in Table. I, the Bode diagram of the closed-loop transfer functions $G_{cref\_c}(s)$ are shown in Fig. 7. It can be concluded from Fig.7 that the magnitude response varies in the vicinity of zero at low frequency range when PI controller is used. Increasing the proportional gain of the PI controller may force the magnitude response approaching zero. However, large gain could cause the control system unstable. The current tracking capability is improved when the Quasi-PR controller is used. The steady state current tracking error is reduced by Quasi-PR controller according to the magnitude and phase response in Fig. 7. Thus, the Quasi-PR controller is a more suitable candidate than PI controller for the precisely controlled CGCI.

The Bode diagram of closed-loop transfer functions $G_{vs\_c}(s)$ are shown in Fig. 8. Results indicate that both two control methods provide enough attenuation to the disturbance from the grid-side voltage. That is to say, the distortion component in the grid-side voltage will not be amplified by the CGCI. Even its coupling circuit is a second LC branch. While for the current control system using PI controller it cannot offer zero dB magnitude gain and zero degree phase shift.

IV. Simulation

A. Simulation setting

TABLE. I PARAMETERS SELECTED FOR MATLAB SIMULATION

Parameters	Value
Switching frequency f_s	10kHz
Fundamental frequency	50Hz
Filter inductor L_C	4mH
Filter capacitor C_C	125uF

In order to verify the effectiveness of the Quasi-PR controller, a set of tests are carried out by PSCAD/EMTDC. For comparison, PI controller with carrier-based PWM is studied in the simulations. Table. II lists the simulated system parameters, and the DC-link voltage of the inverter is supplied by an ideal DC voltage source.

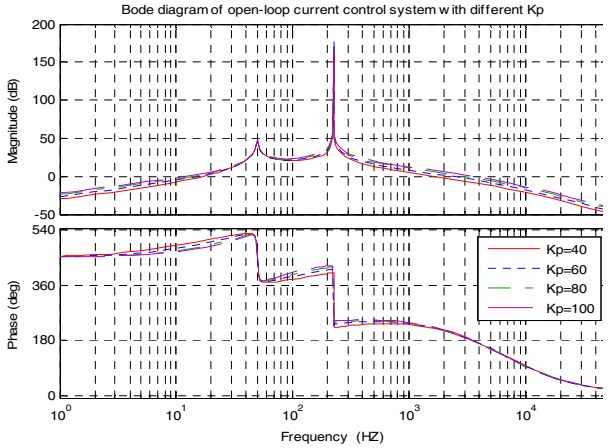

Fig. 5 Bode diagram of open-loop current control system-- $G_{Quasi\text{-}PR}(s)$ $G_{PWM}(s)G_{Imp}(s)$. Parameters: ω_c=5, K_r=5000;

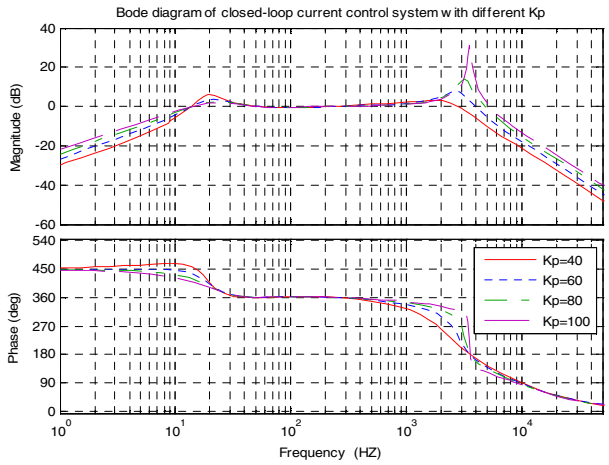

Fig. 6 Bode diagram of closed-loop current control system-- $G_{cref\_c}(s)$ Parameters: Kr=5000, ωc=5;

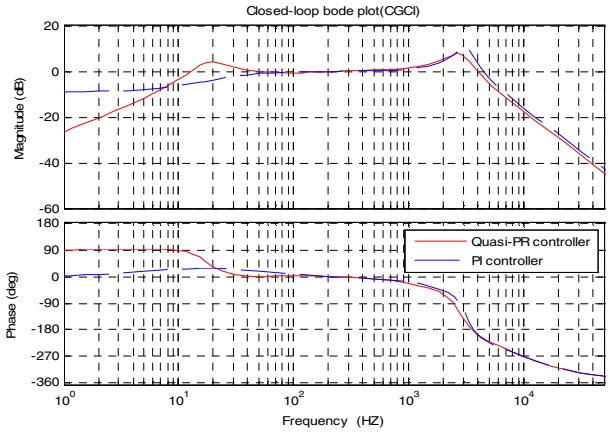

Fig. 7 Bode diagram of closed-loop transfer function $G_{cref\_c}(s)$ (solid line: use

PI controller; dashed line: use Quasi-PR controller)

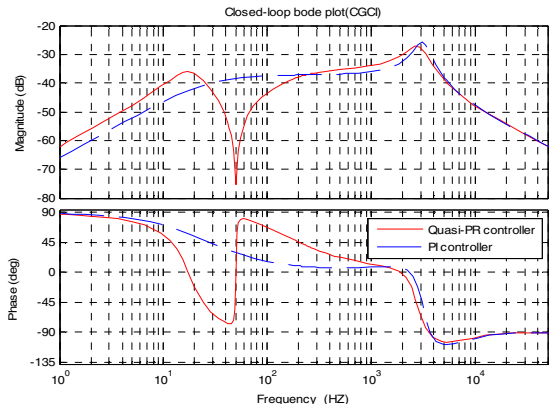

Fig. 8 Bode diagram of closed-loop transfer functions $G_{vs\_c}(s)$ (solid line: use PI controller; dashed line: use Quasi-PR controller)

The comparison is mainly focused on the steady state performance. Thus the performances are conducted with respect to the following performance parameters:

- Source current THD (THD_is) at steady state situation.
- Active power error (P_error) between the injecting active power (P_inj) and the reference active power (P).
- Reactive power error (Q_error) between the injecting reactive power (Q_inj) and the reference reactive power based on the load reactive power (Q_load).

According to Part II, a set of parameters of the Quasi-PR controller can be gotten: K_p=50, ω_c =5, K_r=5800.

TABLE. II SYSTEM SETTING IN THE SIMULATION

System parameters	
Grid Parameters	***Value***
Grid Voltage Vs	220V
fundamental frequency f_0	50Hz
Sampling frequency	20 KHz
Source Inductor Ls	0.001mH
Inverter parameters	***Value***
DC link capacitor C_{DC}	1mF
Filter inductor L_C	4mH
Filter capacitor C_C	125uF
Linear load	
DC link voltage V_{DC}	170V
Linear Load 1（0.5s-0.7s）	15 ohm;0.12 H, 8 ohm
Linear Load 2（0.1s-0.3s）	20 ohm;0.06 H, 10 ohm
Linear Load 3（0.3s-0.5s）	28 ohm;0.04 H, 8 ohm

B. PSCAD Simulation results

Simulation results using PI controller with carrier-based PWM and using Quasi-PR controller with carrier-based PWM respectively are shown in Fig. 9 to Fig. 11, respectively. The system performance indexes are summarized in TABLE. *III* to TABLE. *IV* respectively. It can be concluded that PI controller with carrier-based PWM cannot eliminate the steady state current tracking errors. As a result, both active and reactive power output of the CGCI are not able to tracking the reference with high accuracy. In general, the parameters of the PI controller can be tuned to improve the performance. As shown in Fig. 7, tuning the parameters cannot reduce the source current THD and the power error at the same time.

When Quasi-PR controller with Carrier-based PWM is used, the active power from the external source can be injected to the grid and the load side reactive power is compensated. Both errors are very small. What's more, the low source current THD (<2%) and low power error indicate that the Quasi-PR controller is more fit for applying to CGCI. It can be concluded that Quasi-PR controller with Carrier-based PWM is a better choice for the CGCI structure to achieve active power and reactive power injecting as well as harmonic compensation.

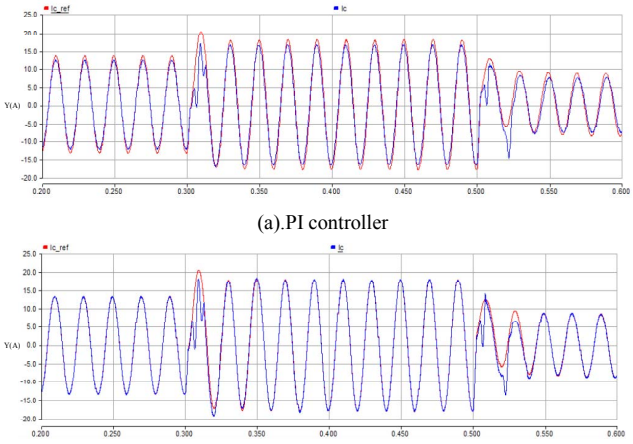

(a).PI controller

(b).Quasi-PR controller

Fig. 9 Current waveforms when load (linear load) changes

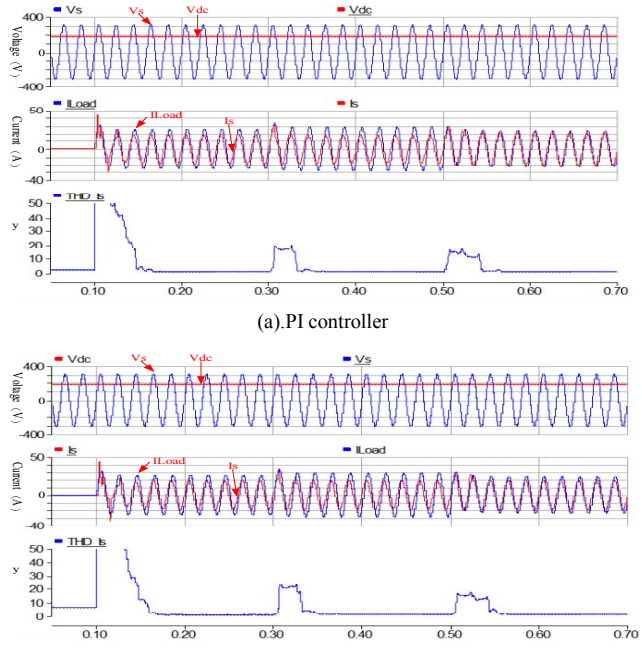

(a).PI controller

(b).Quasi-PR controller

Fig. 10 Voltage and current waveforms & source current THD when load (linear load) changes

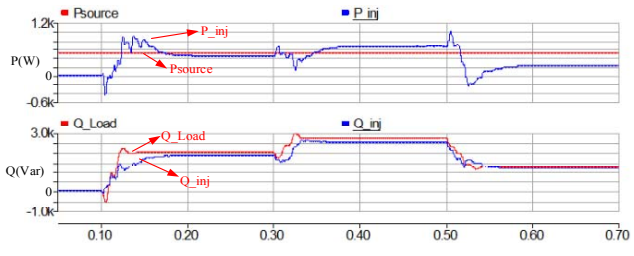

(a).PI controller

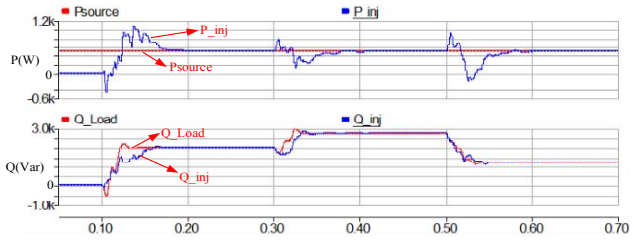

(b).Quasi-PR controller

Fig. 11 Active power and reactive power when load (linear load) changes

TABLE. III STEADY STATE PERFORMANCES UNDER DIFFERENT LOADS SITUATION USING PI CONTROLLER

Steady State(Linear Load)--PI controler (Kp=72，Ki=4500)							
Time	***THD_is***	***P_inj***	***P***	***Q_inj***	***Q_load***	***P_error (%)***	***Q_error (%)***
0.29s	0.95	439.39	500	1855.86	2002.29	12.12	7.31
0.49s	1.09	659.07	500	2510.47	2738.77	31.81	8.34
0.69s	1.10	214.17	500	1178.07	1227.64	57.17	4.04

TABLE. IV STEADY STATE PERFORMANCES UNDER DIFFERENT LOADS SITUATION USING QUASI-PR CONTROLLER

Steady State(Linear Load)--Quasi-PR controller (Kp=50，Wc=5，Kr=5800)							
Time	***THD_is***	***P_inj***	***P***	***Q_inj***	***Q_load***	***P_error (%)***	***Q_error (%)***
0.29s	0.84	500.12	500	2021.64	2002.3	0.02	0.97
0.49s	0.99	499.94	500	2761.53	2738.78	0.01	0.83
0.69s	1.02	482.22	500	1257.3	1227.64	3.56	2.42

V. EXPERIMENT RESULTS

TABLE. V EXPERIMENTAL SYSTEM SETTINGS

Items	**Value**
Capacitor Cc	120.95uF
Inductor Lc	3.791uH(1kHz)
Grid Voltage Vs	110Vrms,50Hz
DC-link Voltage	85 Volt
Active power transfer	90W
Linear Load	14ohm,25.27mH

A lab-scale prototype, with parameters listed in *TABLE. V*, was constructed. The control algorithm was implemented in a DSP-TMS320F28335. The photo of the prototype is shown in Fig. 12. The grid-side voltage is drop to 110V due to the laboratory safety reason and the fact that 110V grid voltage is also used by many countries such as America, Japan and Canada. The parameters (K_p=50, ω_c=5, K_r=5800) designed by the proposed parameters design approach was used in the experiment.

As stated previously, the comparison are mainly focused on the steady state performance. Thus the performances are conducted with respect to the following performance parameters:

- Source current THD at steady state situation.
- Active power error between the injecting active power and the reference active power.
- Reactive power error between the injecting reactive power and the reference reactive power based on the load reactive power, in the experiment, it can be simply regarded as the source side reactive power.

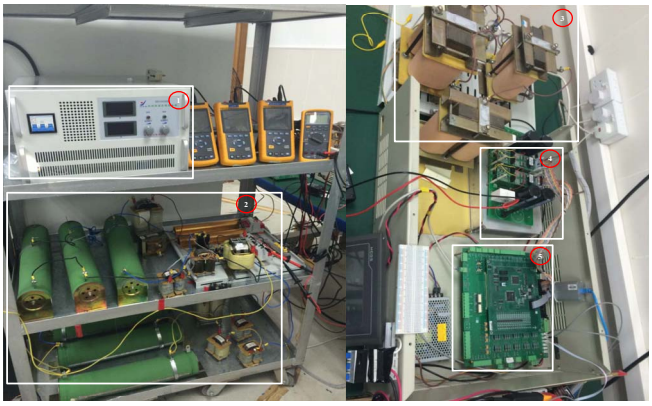

Fig. 12 Experimental Prototype (Note: ①-DC power supply; ②-Loads; ③-Coupling impedance; ④-IGBT and drivers; ⑤-Control board and signal conditional circuit.)

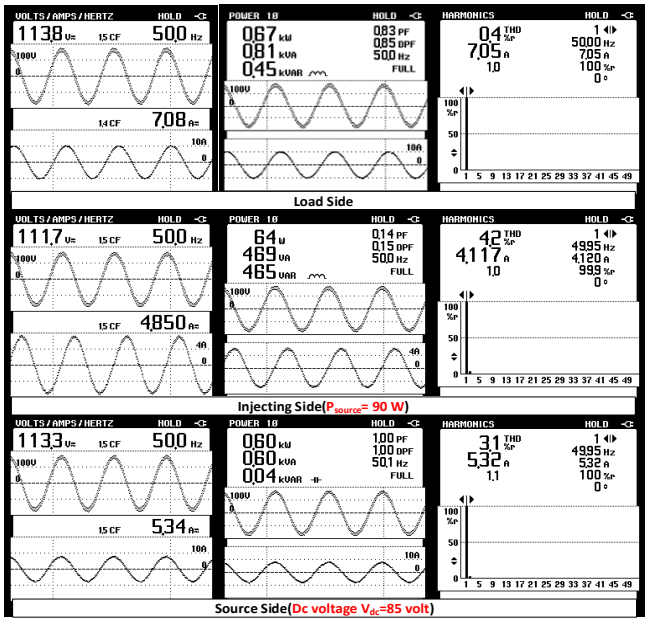

Fig. 13 Experimental results of PI controller with carrier-based PWM

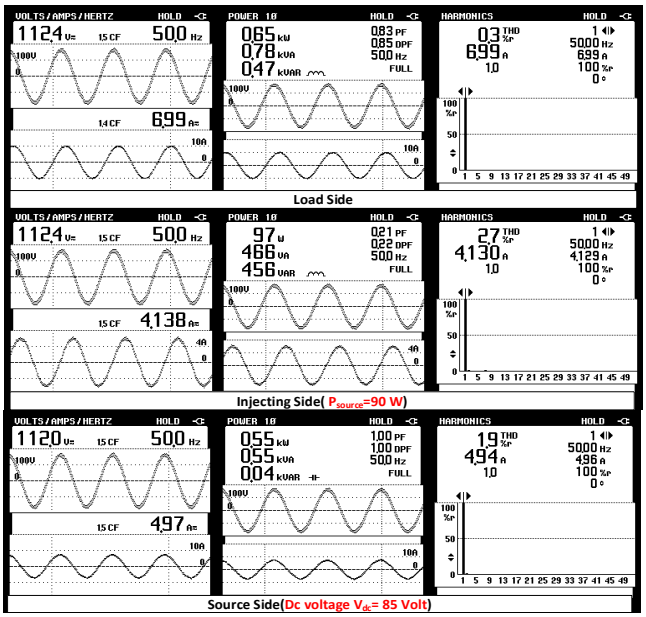

Fig. 14 Experimental results of Quasi-PR controller with carrier-based PWM

TABLE. VI EXPERIMENTAL RESULTS

	Load Side			Source Side		Power			
	PF	Q (Var)	THD (Load)	THD	PF	P_ref (W)	P_actual (W)	P_Error (W)	Q_source (Var)
PI	0.83	450	0.4	3.1	1.00	90	64	26	40
PR	0.83	456	0.3	1.9	1.00	90	97	7	40

[a] Note: PI—PI controller with carrier-based PWM; PR—Quasi-PR controller with carrier-based PWM; P_ref—active power generated by distributed generators; P_actual—active power injecting to the grid; P_error—Error between P_ref and P_actual; Q_source—reactive power exists in the source side and it is the reactive power error between injecting reactive power and load side reactive power.

When the DC voltage is 85V, which is lower than the grid side voltage 110V, and the active power range is set as 90W, a linear inductive load is used to verify the current control performance of Quasi-PR controller with carrier-based PWM. Comparison experiments are conducted by using PI controller with carrier-based PWM. The results are given in Table. VI. Fig. 13 shows the experimental results (load side, injecting side and source side) when PI controller with carrier-based PWM was used and P_{source} equals to 90W. Fig. 14 shows the experimental results when Quasi-PR controller was applied and P_{source} equals to 90W. It indicates from those experimental results that compared to PI controller with carrier-based PWM, power error between reference value and actual value can be reduced and source current THD can be decreased by using Quasi-PR controller with carrier-based PWM, which shows the effectiveness of the proposed current control model and parameters design of Quasi-PR controller.

VI. CONCLUSION

The capacitive-coupling grid-connected inverter can decrease DC-link voltage and running losses. While due to its second-order transfer function of capacitive-coupling interfacing branch, the mathematical model and current controller for traditional IGCI cannot be directly applied to CGCI. This paper proposes a Quasi-PR controller with carrier-based PWM for CGCI and its related Quasi-PR controller parameters design method. Both simulation and experimental results are provided. Comparison with PI controller is also given to validate the effectiveness of proposed model and parameters design approach. Results shows that the Quasi-PR controller with carrier-based PWM is a better choice to fulfill the requirements of active power and reactive power injecting as well as harmonic compensation.

ACKNOWLEDGMENT

The authors would like to thank the Science and Technology Development Fund, Macao SAR Government with the project (072/2012/A3) and University of Macau with the project (MYRG2015-00084-FST) for their financial support.

REFERENCES

[1] V. K. N. Lau and D. H. K. Tsang, "Optimal Energy Scheduling for Residential Smart Grid With Centralized Renewable Energy Source," IEEE Syst. J., vol. 8, no. 2, pp. 562–576, Jun. 2014.

[2] C. K. Lee, B. Chaudhuri, and S. Y. Hui, "Hardware and Control Implementation of Electric Springs for Stabilizing Future Smart Grid With Intermittent Renewable Energy Sources," IEEE J. Emerg. Sel. Top. Power Electron., vol. 1, no. 1, pp. 18–27, Mar. 2013.

[3] V. Salehi, A. Mohamed, A. Mazloomzadeh, and O. A. Mohammed, "Laboratory-Based Smart Power System, Part I: Design and System Development," IEEE Trans. Smart Grid, vol. 3, no. 3, pp. 1394–1404, Sep. 2012.

[4] A. Izadian, N. Girrens, and P. Khayyer, "Renewable Energy Policies: A Brief Review of the Latest U.S. and E.U. Policies," IEEE Ind. Electron. Mag., vol. 7, no. 3, pp. 21–34, Sep. 2013.

[5] H. Calleja and H. Jimenez, "Performance of a grid connected PV system used as active filter," Energy Convers. Manag., vol. 45, no. 15–16, pp. 2417–2428, Sep. 2004.

[6] Z. Zeng, H. Yang, R. Zhao, and C. Cheng, "Topologies and control strategies of multi-functional grid-connected inverters for power quality enhancement: A comprehensive review," Renew. Sustain. Energy Rev., vol. 24, pp. 223–270, Aug. 2013.

[7] X. Zhang, J. W. Spencer, and J. M. Guerrero, "Small-Signal Modeling of Digitally Controlled Grid-Connected Inverters With LCL Filters," IEEE Trans. Ind. Electron., vol. 60, no. 9, pp. 3752–3765, Sep. 2013.

[8] W. Wu, Y. He, and F. Blaabjerg, "An LLCL Power Filter for Single-Phase Grid-Tied Inverter," IEEE Trans. Power Electron., vol. 27, no. 2, pp. 782–789, Feb. 2012.

[9] Z. Zou, Z. Wang, and M. Cheng, "Modeling, Analysis, and Design of Multifunction Grid-Interfaced Inverters With Output LCL Filter," IEEE Trans. Power Electron., vol. 29, no. 7, pp. 3830–3839, Jul. 2014.

[10] Wen-Chen Zhang, Ning-Yi Dai, and Man-Chung Wong, "Capacitive-coupled grid-connected inverter with active power injection ability," in Proceedings of The 7th International Power Electronics and Motion Control Conference, 2012, vol. 3, pp. 1639–1645.

[11] Ning-Yi Dai, Wen-Chen Zhang, Man-Chung Wong, J. M. Guerrero, and C.-S. Lam, "Analysis, Control and Experimental Verification of a Single-Phase Capacitive-Coupling Grid-Connected Inverter," IET Power Electron., 2014.

[12] S. Ostroznik, P. Bajec, and P. Zajec, "A Study of a Hybrid Filter," IEEE Trans. Ind. Electron., vol. 57, no. 3, pp. 935–942, Mar. 2010.

[13] L. Herman, I. Papic, and B. Blazic, "A Proportional-Resonant Current Controller for Selective Harmonic Compensation in a Hybrid Active Power Filter," IEEE Trans. Power Deliv., vol. 29, no. 5, pp. 2055–2065, Oct. 2014.

[14] Wen-Chen Zhang, Ning-Yi Dai, and Man-Chung Wong, "Capacitive-coupled grid-connected inverter with active power injection ability," in Proceedings of The 7th International Power Electronics and Motion Control Conference, 2012, vol. 3, pp. 1639–1645.

[15] C.-S. Lam, W.-H. Choi, M.-C. Wong, and Y.-D. Han, "Adaptive DC-Link Voltage-Controlled Hybrid Active Power Filters for Reactive Power Compensation," IEEE Trans. Power Electron, vol. 27, no. 4, pp. 1758–1772, Apr. 2012.

[16] F. Blaabjerg , R. Teodorescu , M. Liserre and A. V. Timbus "Overview of control and grid synchronization for distributed power generation

systems", IEEE Trans. Ind. Electron., vol. 53, no. 5, pp.1398 -1409 2006

[17] S. Yang, Q. Lei, F. Z. Peng, and Z. Qian, "A Robust Control Scheme for Grid-Connected Voltage-Source Inverters," IEEE Trans. Ind. Electron., vol. 58, no. 1, pp. 202–212, Jan. 2011.

[18] Z. Yao and L. Xiao, "Control of Single-Phase Grid-Connected Inverters With Nonlinear Loads," IEEE Trans. Ind. Electron., vol. 60, no. 4, pp. 1384–1389, Apr. 2013.

[19] M. P. Kazmierkowski and L. Malesani, "Current control techniques for three-phase voltage-source PWM converters: a survey," IEEE Trans. Ind. Electron., vol. 45, no. 5, pp. 691–703, 1998.

[20] F. Briz, M. Degner, and R. Lorenz, "Dynamic analysis of current regulators for AC motors using complex vectors," IEEE Trans. on Ind. App., vol. 35, no. 6, pp. 1424-1432, Nov/Dec 1999.

[21] D. N. Zmood and D. G. Holmes, "Stationary frame current regulation of PWM inverters with zero steady-state error," IEEE Trans. Power Electron., vol. 18, no. 3, pp. 814–822, May 2003.

[22] E. Twining and D. G. Holmes, "Grid current regulation of a three-phase voltage source inverter with an LCL input filter," IEEE Trans. Power Electron., vol. 18, no. 3, pp. 888–895, May 2003.

[23] D. N. Zmood and D. G. Holmes, "Stationary frame current regulation of PWM inverters with zero steady-state error," IEEE Trans. Power Electron., vol. 18, no. 3, pp. 814–822, May 2003.

[24] K. H. Ahmed, A. M. Massoud, S. J. Finney, and B. W. Williams, "A Modified Stationary Reference Frame-Based Predictive Current Control With Zero Steady-State Error for LCL Coupled Inverter-Based Distributed Generation Systems," IEEE Trans. Ind. Electron., vol. 58, no. 4, pp. 1359–1370, Apr. 2011.

[25] J. M. Guerrero, J. Matas, L. Garcia de Vicuna, N. Berbel, and J. Sosa, "Wireless-Control Strategy for Parallel Operation of Distributed Generation Inverters," in Proceedings of the IEEE International Symposium on Industrial Electronics, 2005. ISIE 2005., 2005, vol. 2, pp. 845–850.

[26] D. M. Van de Sype, K. De Gusseme, A. P. Van den Bossche, and J. A. Melkebeek, "Small-signal Laplace-domain analysis of uniformly-sampled pulse-width modulators," in 2004 IEEE 35th Annual Power Electronics Specialists Conference (IEEE Cat. No.04CH37551), 2004, vol. 6, pp. 4292–4298.

[27] D. Maksimovic and R. Zane, "Small-Signal Discrete-Time Modeling of Digitally Controlled PWM Converters," IEEE Trans. Power Electron., vol. 22, no. 6, pp. 2552–2556, Nov. 2007

[28] Pan Geng, Weimin Wu, Yinzhong Ye, and Yijian Liu, "Small signal modeling of a novel single-phase photovoltaic inverter," in 2009 IEEE 6th International Power Electronics and Motion Control Conference, 2009, pp. 2188–2192.

[29] X. Zhang, J. W. Spencer, and J. M. Guerrero, "Small-Signal Modeling of Digitally Controlled Grid-Connected Inverters With LCL Filters," IEEE Trans. Ind. Electron., vol. 60, no. 9, pp. 3752–3765, Sep. 2013.

[30] A. Khairy, M. Ibrahim, N. Abdel-Rahim, and H. Elsherif, "Comparing proportional-resonant and fuzzy-logic controllers for current controlled single-phase grid-connected PWM DC/AC Inverters," in IET Conference on Renewable Power Generation (RPG 2011), 2011, pp. 153–153.

[31] D. N. Zmood and D. G. Holmes, "Stationary frame current regulation of PWM inverters with zero steady state error," in 30th Annual IEEE Power Electronics Specialists Conference. Record. (Cat. No.99CH36321), 1999, vol. 2, pp. 1185–1190.